TECHNICAL ARTICLE—PEER-REVIEWED

Elaeocarpus Seed Extraction and Their Impact as a Corrosion Inhibitor for Mild Steel Submerged in HCl Wash Solution: Insight from Experimental, Mathematical, and Theoretical Views

Narasimha Raghavendra · B. E. Kumaraswamy

Abstract Herein, Elaeocarpus seed (ES) extract was studied in 3 M HCl solution as a efficacy corrosion inhibitor for the mild steel through mass loss, electrochemical Tafel diagrams, impedance spectroscopy, atomic absorption spectroscopy, scanning electron microscopy, and EDX techniques. During weight loss technique, it is observed that increasing the concentration enhances the protective role of the plant product. The Tafel diagrams showed a mixed role of the ES extract. In impedance spectroscopy, the area of depressed semicircle has a direct relationship with the plant extract concentration, which clearly demonstrating the inhibition property of ES extract. 93.370, 97.111, 89.015, and 90.528% are the maximum inhibition efficiencies obtained from the weight loss, atomic absorption spectroscopy, Tafel plot, and impedance spectroscopy techniques, respectively. Mathematical and quantum chemical studies further support the experimental results.

N. Raghavendra (✉)
Department of Chemistry, K.L.E. Society's P. C. Jabin Science College (Autonomous), Vidyanagar, Hubballi 580031, India
e-mail: rcbhat3@gmail.com

B. E. Kumaraswamy
Department of Industrial Chemistry, Kuvempu University, Jnanasahyadri, Shankaraghatta, Shivamogga Dist., Karnataka 577451, India

Graphic abstract
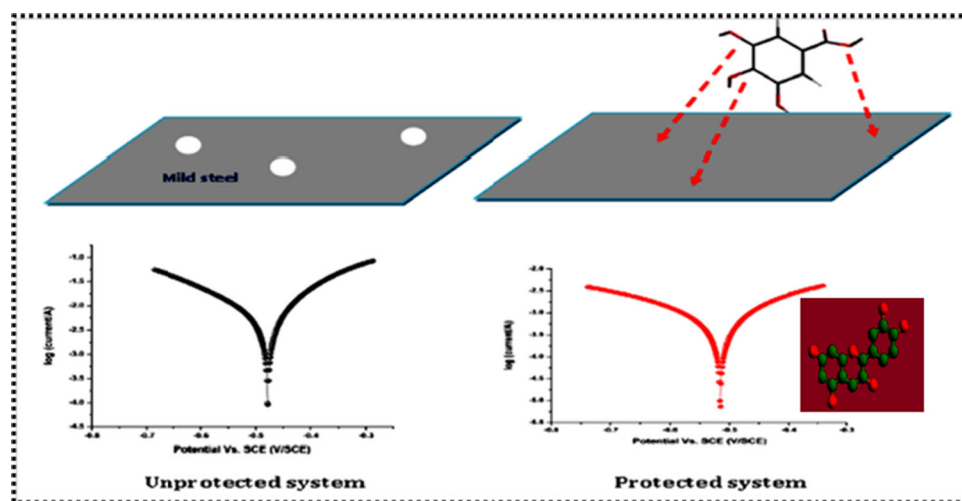
Introduction

Mild steel (MS) is an important metal and commonly used in various human and industrial activities. Hence, nowadays application of MS metal in industries has increased. The MS has good standard corrosion potential, innocuousness, high stiffness, high electrical conductivity, and light weight. Because of these properties, MS metal is used in packing, transportation, chemical, and engineering applications. The MS metal often contacts corrosive ions (H^+ or Cl^-) in various industrial processes. The exposed MS metal loses its weight due to the aggressive attack of corrosive ions. These corrosive solutions increase the dissolution process by destroying the MS surface [1–5].

Corrosion of MS not only affects the properties of the metal, but also affects the nation's economy. Hence, prevention of MS corrosion is very much essential. Among the corrosion inhibiting process, chemical inhibitors are the best choice owing to the strong adsorption property. In past decades, several inorganic inhibitors such as nitrites, phosphates, molybdates, tungstate's, silicates, and chromates have been found to serve as effective potential corrosion inhibitors for a variety of metallic systems, by repressing both the cathodic and anodic reactions. In addition, a majority of polymeric and organic species showed the predominant anticorrosive behavior at the metal–electrolyte solution interface.

Organic species bearing special elements such as N, O, S, and P, the pi electrons in the conjugated double/triple bonds and individual functional groups in their moieties are assigned as good adsorption centers show good inhibitive action by shifting the electrons via pi orbitals by on adsorption mechanism. The adsorption process leads to modification in the electrochemical process in the region of the double layer. Adsorption occurs when the liquid species accumulate on the solid surface, which is due to the presence of an invisible thick layer on the surface of a solid. It is applicable in the chemical, physical, and biological processes. It is operative in the various industrial operations such as purification of water, activated charcoal, and synthetic resins.

The adsorption takes place in two ways, (a) physical force adsorption (occurs through weak Van der Waals forces) and (b) chemical force adsorption (occurs through formation of a new chemical bond between adsorbent and adsorbate). The adsorption process mainly depends upon several factors such as, the nature of the metal, metal surface charge, type of electrolyte solution, molecular configuration in the inhibitor and nature of interaction of inhibitor molecules on the surface of the metal [6–9]. The artificial corrosion inhibitors such as Nicotinamide, acetylenic alcohols, and thiourea are mainly employed in pickling, descaling, etching, electrochemical, and chemical processes. Many industries have strictly banned these synthetic compounds because of their toxicity nature. Therefore, research shifted toward cheap and eco-friendly corrosion inhibitors. Plant products fulfill these characteristics [10–12].

Ekanem et al. [13] selected *Pineapple leaves* and examined their role as green corrosion inhibitor on MS

960

J Fail. Anal. and Preven. (2021) 21:958–975

surface in HCl medium via chemical technique. They reported good protection efficiency of the plant extract. Langmuir adsorption model was the best fit for their study. Authors, Hussin and Kassim [14] tested the influence of *Uncaria Gambir* plant extract on MS in hydrochloric acid. Protection efficiency of *Uncaria Gambir* plant extract was due to adsorption of green chemicals from the plant extracts on the surface of the MS which followed the Langmuir isotherm model. Ambrish Singh et al. [15] selected electrochemical and chemical techniques to examine the corrosion inhibition role of *Karanj* seed extract on MS surface in HCl medium. Weight loss studies show that protection efficiency increased with plant extract concentration. Ji et al. [16] discussed the activities of *Argemone Mexicana* extract on the surface of the MS in HCl environment by employing UV-visible, surface imaging, and electrochemical techniques.

Even though there are many reports available on MS corrosion inhibition in the literature, further research is required in order to solve the MS dissolution process in industries. Hence, in the present research, we selected Elaeocarpus seed. Literature study confirms that Elaeocarpus seed contains alkaloids, glycosides, saponins, phenolic compounds, tannins, phytosterols, carbohydrates, proteins, aminoacids, flavanoids, quinones, and terpenoids [17, 18]. The presence of functional groups in green extract was analyzed by FT-IR spectroscopy. The adsorption and corrosion inhibition properties of Elaeocarpus seed extract was examined by weight loss, electrochemical (Tafel plot and AC impedance), and atomic absorption spectroscopy techniques. Further, mathematical model and quantum studies used to support the experimental results.

Experimental Section

Preparation of Optimum Concentration (OC) of Corrosion Inhibitor

About 300 g of the Elaeocarpus seed (ES) was crushed and soaked in half liter of 1% aqueous hydrochloric acid solution for one day at temperature 303 K. Green chemicals present in the Elaeocarpus seed were extracted with the help of Soxhlet extractor. The solution filtered and kept in a refrigerator in order to prevent its degradation.

Attempts were successfully made to determine the optimum concentration (OC) by preparing different amounts of Elaeocarpus seed (ES) extract. The amount (A_{ESE}) of a given ESE concentration (C_{ESE}) added to HCl solution (V_{HCl}) was analyzed through the following relation:

$$A_{ESE} = \frac{V_{HCl}C_{ESE}}{10^{-6}} \qquad (Eq\ 1)$$

It was observed that Elaeocarpus seed extract (ESE) amount between 5 to 8 mg/L yields same protection efficiency values. Below this, the protection efficiency increases with a rise in the ESE concentration. Above this, no significant variations in the protection values were observed. This was true for five different solution temperatures (303, 313, 323, 333, and 343 K). Hence, from these it was decided to use concentrations of ES extract selected within 1–5 mg/L at five different solution temperatures. Five different concentrations, namely 1, 2, 3, 4, and 5 mg/L were made for chemical, electrochemical, and surface studies.

Phytochemical, Physical Parameters, and Functional Groups Screening

Phytochemical tests were performed to determine the bioactive species such as alkaloids, polyphenols, tannins, and saponins present in the Elaeocarpus seed. The tests were carried out according to the procedure reported in the literature [19]. To support phytochemical and FT-IR results, physical parameters (refractive index (n_{D20}), surface tension (dynes/cm), viscosity (centipoise), and density (g/ml)) were determined and tabulated in Table 1.

Materials and Chemicals

The MS metal pieces with chemical composition (weight %): Mn = 0.6, C = 0.18, P = 0.04, S = 0.05, Si = 0.1, and Fe = 99.03 were employed for experimental tests. About 3 M HCl solution was prepared by using double distilled water.

Thermal Properties

The thermal properties of Elaeocarpus seed extract at different stages were performed by analyzing the 10 mg samples. The weight derivative, heat flow rate, and weight loss were determined by using differential thermal analysis (DTA), differential scanning calorimetry (DSC), and thermo gravimetric analysis (TGA), respectively, with the help of a thermogravimetric analyzer (Model; SDT Q600 V20.9, Japan). The tests were performed under dry N_2 gas atmosphere with a flow rate of 30 ml/min from room temperature to 400 °C. DSC measures the heat flow rate

Table 1 Physical parameters of Elaeocarpus seed extract

Refractive Index (n_{D20})	Surface tension (dynes/cm)	Viscosity (centipoise)	Density (g/ml)
1.546	93.457	1.0345	1.324

with respect to the temperature giving information on molecular transformations such as phase changes. All these three techniques provide information about how material changes under thermal conditions.

Gravimetric Experiment

In the weight loss technique, initial weight of the MS was taken prior to test by using an analytical balance. The MS

$$\theta = \frac{\text{Weight of MS dissolved in unprotected condition} - \text{Weight of MS dissolved in protected condition}}{\text{Weight of MS dissolved in unprotected condition}}$$

pieces were introduced to 3 M HCl solution separately without and with different amounts of green compounds for 2, 4, 6, 8, and 10 h at 303 K. The experiments were also

$$PE = \frac{\text{Weight of MS dissolved in unprotected condition} - \text{Weight of MS dissolved in protected condition}}{\text{Weight of MS dissolved in unprotected condition}} \times 100.$$

carried out at 313, 323, 333, and 343 K at immersion period of 2 h. After the specified time, MS specimens are withdrawn from the acid solution. The difference in the MS weight was recorded. The corrosion rate (CR), degree of surface coverage (θ), and inhibition efficiency (IE%) were calculated using equations 2, 3, and 4.

$$CR = \frac{W}{At} \qquad (Eq\ 2)$$

$$\theta = \frac{(CR_1 - CR_2)}{CR_1} \qquad (Eq\ 3)$$

$$IE(\%) = \frac{(CR_1 - CR_2)}{CR_1} \times 100, \qquad (Eq\ 4)$$

where W = average MS weight loss (mg), A = MS area in cm^2, T = exposed time in hours, CR_2 = corrosion rate values in the presence green compounds and CR_1 = corrosion rate values in the absence of green compounds.

Atomic Absorption Spectroscopy (AAS) Evaluation

The AAS experiment provides important information about concentration of the ionic species on the sample surface. Generally, the concentration of ionic species decreases with respect to concentration of the inhibitor molecules.

Hence, in present investigation, AAS test performed in 100 ml of 3 M HCl solution without and with five different concentrations of ES extract (1, 2, 3, 4, and 5 mg/L) on mild steel surface at 303 K with an exposure period of two hours. For this purpose, AAS analyzer of model G8-908 (Australia) was used. The AAS test performed three times and average values are reported.

The surface coverage (θ) was evaluated with the help of the following relation:

The protection efficiency (PE) was calculated from the below equation:

Electrochemical Studies

Conventional platinum (auxiliary), calomel (reference) and MS (working) electrodes were used to carry out the Tafel and AC impedance studies. Tafel diagrams were obtained in ± 200 mV potential range at a scan rate of 0.01 V/s. Nyquist plot were obtained in the frequency range 1,000,000–1 Hz with an AC signal of 0.01 V. The schematic representation of electrochemical cell shown in Figure 1.

Mathematical and Quantum Chemical Studies

In this investigation, the weight loss results at different times and temperatures can be studied through mathematical models. Further, the different Quantum chemical parameters, i.e., energy of lowest unoccupied molecular orbital (E_{LUMO}), energy of highest occupied molecular orbital (E_{HOMO}), electro negativity (χ), electrophilicity index (ω), chemical hardness (η), Chemical softness or electron polarizability (σ), electron affinity (A), chemical potential (μ), ionization potential (I) were calculated from the ArgusLab software as per the previous report [20].

962

J Fail. Anal. and Preven. (2021) 21:958–975

Results and Discussion

Fourier Transform-Infrared (FT-IR) Analysis

The functional groups in the Elaeocarpus seed extract were identified through FT-IR spectroscopic technique. Fig. 2 shows the IR spectrum of Elaeocarpus seed extract. The likely available groups in the Elaeocarpus seed extract are presented in the figure. The electron-rich groups are expected to participate in the adsorption process and generate a protective film on the substrate surface in acid media, which effectively isolate the substrate surface from the corrosive solution.

Phytochemical Results

The phytochemical species present in the results Elaeocarpus seed extract are reported in Table 2. It is observed that the Elaeocarpus seed extract mainly contains polyphenols, tannins and flavonoids in their moieties. These constituents contain hydroxyl (OH) and carbonyl (C=O) groups, which accelerate the adsorption process, thus increasing the protection ability of Elaeocarpus seed extract. Our previous studies also attributed the protection property of plant extract species to presence of these bioactive species [21].

Thermal Properties

Thermal gravimetry is the study of material nature as a function of temperature. Thermogravimetry gives important information about the decomposition profile of plant extract constituents and its kinetic properties. Previously, many scientists reported that the decomposition of plan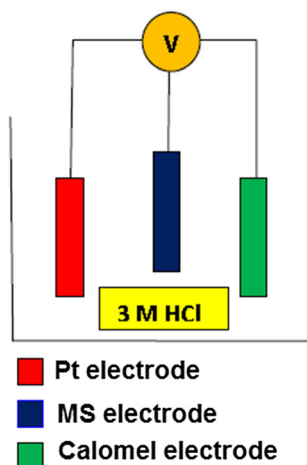t extract constituents with respect to temperature follows first order kinetics. Hence, decomposition of plant extract constituents is directly proportional to the concentration of its individual species. The literature study shows that Elaeocarpus seed extract mainly contains alkaloids, polyphenols, and tannins in their moiety. The detailed results of thermal properties carried out on Elaeocarpus seed extract are shown in Figure 3a, b, and c.

From TGA Figure 3a and DTG Figure 3b, the initial weight loss occurs at 30 °C and continues up to 110 °C, which is due to evaporation of moisture content in the Elaeocarpus seed extract, decomposition of some lower melting point species and intermolecular hydrogen bonded chemical adsorbed water species. The next degradation occurs at 240 °C which is due to decomposition of catechin, epicatechin, gallic acid, tannic acid, and ellagic acid. The DTG (Fig 3b, shows one broad exothermic peak at 268 °C, which is an indication of decomposition of gallic acid, it contains oxygen functional groups.

DSC Fig 3c shows heat flow rate with respect to temperature change. From all these, it is concluded that, Elaeocarpus seed extract contains a high concentration of gallic acid, tannic acid, and ellagic acid which are expected to participate in the corrosion process. The chemical structure of important constituents presents in the Elaeocarpus seed extract are shown in Figure 4.
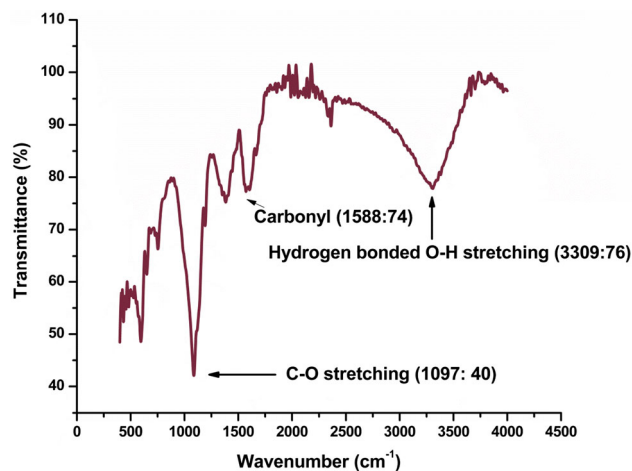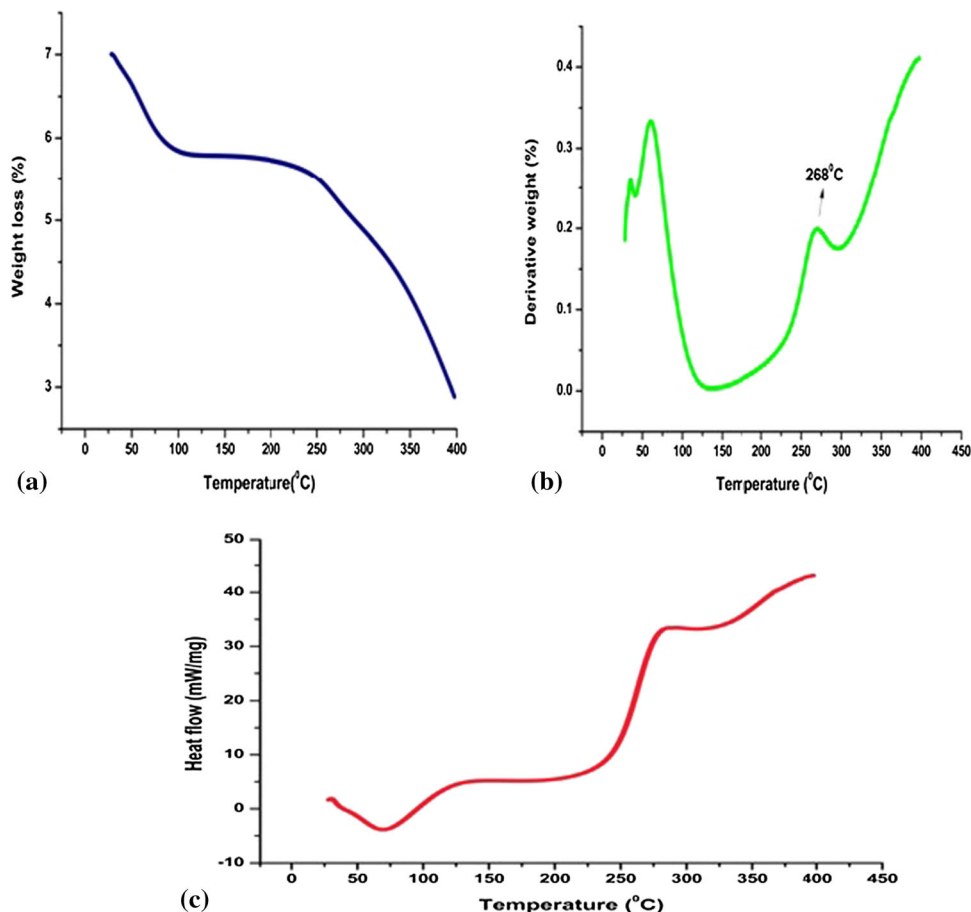

Fig. 2 IR spectrum of Elaeocarpus seed extract

Table 2 Phytochemical screening results of Elaeocarpus seed extract

Polyphenols	Tannins	Flavonoids	Alkaloids	Saponin
+	+	+	+	−

+, present; −, absent

Fig. 1 Schematic representation of electrochemical cell

Fig. 3 TGA (**a**), DTA (**b**), and DSC (**c**) of Elaeocarpus seed extract


Weight Loss Experiment

The weight loss test was carried out at five different solution temperatures to study the influence of ES extract concentration, contact time, and solution temperature. The contact time and solution temperature not only influence corrosion rate of MS in 3 M HCl solution, but also influence the interaction between the surface of MS and ES extract. The influence of solution temperature and contact time on the disintegration of MS is abstruse.

The values of corrosion rate, degree of surface coverage and protection efficiency for different green compound concentrations are reported in Tables 3 and 4. The corrosion protection efficiency increases, and corrosion rate decreases sharply with the increase in the concentration of green compounds. This behavior is due to the enhancement in the surface coverage by the green compounds on the MS surface, indicating that the plant extract species exhibits the corrosion inhibition property which reduces the attack of corrosive ions by preventing the attack of H^+ and Cl^- ions on MS surface.
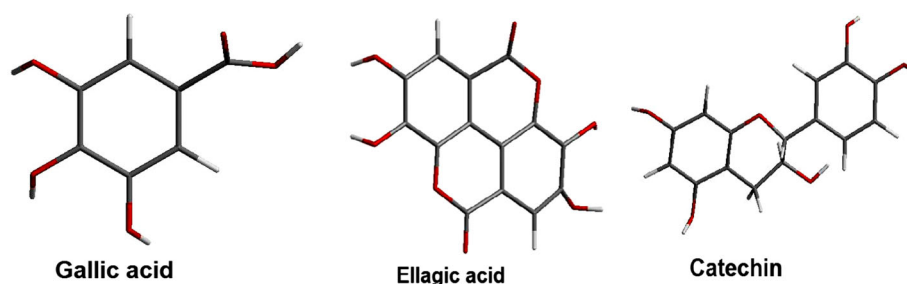
A decrease in the protection efficiency with the increase in time and temperature was observed. The reduction in the inhibition property is correlated to the desorption of green species from the MS surface and corrosion inhibition efficiency of the extract has an inverse relationship with both time and temperature of the system. The enhanced MS dissolution is a complex phenomenon, because at higher solution temperature many modifications take place on the surface of MS such as rapid etching, decomposition, and desorption of plant extract species. The decrease in protection efficiency values with an increase in the solution temperature signifies physisorption.

Plant extract species exhibit corrosion protection due to the formation of a protective layer on metal surfaces via an adsorption process. The adsorption takes place by replacing water species by plant extract active molecules as per the following relation:

$$\text{(Plant extract)}_{(Solution)} + (nH_2O)_{(ads)}$$
$$\rightarrow \text{(Plant extract)}_{(ads)} + nH_2O_{(Solution)}$$
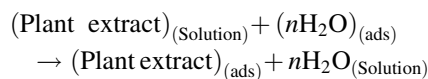
In the present study, ES extract species undergo adsorption on the surface of MS by replacing the water species, which leads to MS-ES extract interaction. The nature of the adsorption process can be studied by introducing weight loss parameters into Freundlisch, Langmuir, Frumkin, Temkin, Flory-Huggins, and Kinetic

964

J Fail. Anal. and Preven. (2021) 21:958–975

Fig. 4 Major constituents of
Elaeocarpus seed extract

Gallic acid   **Ellagic acid**   **Catechin**

Table 3 Weight loss parameters at 303 K

Time (hours)	Concentration (mg/L)	Corrosion rate (mgcm^{-2} h^{-1})	Surface coverage (θ)	Protection efficiency (%)
2	Blank	0.1525		
	1	0.0566	0.6288	62.885
	2	0.0430	0.7179	71.796
	3	0.0310	0.7965	79.652
	4	0.0210	0.8618	86.183
	5	0.0100	0.9337	93.370
4	Blank	0.2743		
	1	0.1153	0.5796	57.965
	2	0.0902	0.6711	67.116
	3	0.0601	0.7808	78.080
	4	0.0491	0.8207	82.070
	5	0.0201	0.9267	92.672
6	Blank	0.4133		
	1	0.2088	0.4947	49.470
	2	0.1803	0.5637	56.370
	3	0.1507	0.6353	63.537
	4	0.1199	0.7098	70.980
	5	0.0601	0.8545	85.458
8	Blank	0.6080		
	1	0.3108	0.4887	48.870
	2	0.2801	0.5391	53.919
	3	0.2301	0.6214	62.141
	4	0.2015	0.6684	66.847
	5	0.1108	0.8176	81.760
10	Blank	0.7991		
	1	0.4310	0.4567	45.676
	2	0.3887	0.5135	51.357
	3	0.3564	0.5530	55.300
	4	0.3071	0.6156	61.560
	5	0.2171	0.7282	72.828

Table 4 Effect of 3 M HCl solution on protection efficiency at different solution temperatures in 2 hours

Temperature (K)	Concentration (mg/L)	Corrosion rate (mgcm^{-2} h^{-1})	Surface coverage (θ)	Protection efficiency (%)
303	Blank	0.1525		
	1	0.0566	0.6288	62.885
	2	0.0430	0.7179	71.796
	3	0.0310	0.7965	79.652
	4	0.0210	0.8618	86.183
	5	0.0100	0.9337	93.370
313	Blank	0.1788		
	1	0.0873	0.5116	51.160
	2	0.0645	0.6390	63.909
	3	0.0513	0.7130	71.300
	4	0.0315	0.8236	82.365
	5	0.0177	0.9009	90.009
323	Blank	0.1901		
	1	0.1031	0.4576	45.760
	2	0.0834	0.5612	56.128
	3	0.0614	0.6768	67.850
	4	0.0410	0.7842	78.427
	5	0.0200	0.8946	89.630
333	Blank	0.2103		
	1	0.1198	0.4303	43.030
	2	0.1031	0.5097	50.970
	3	0.0880	0.5815	58.155
	4	0.0630	0.7004	70.042
	5	0.0380	0.8193	81.930
343	Blank	0.2343		
	1	0.1401	0.4020	40.200
	2	0.1208	0.4844	48.440
	3	0.1001	0.5727	57.270
	4	0.0807	0.6555	65.550
	5	0.0503	0.7853	78.531

thermodynamic adsorption models. The result shows that the correlation coefficient (R^2) between the degree of surface coverage (θ) and concentration (C) of ES extract on MS surface in 3 M HCl solution for the Langmuir model was above 0.9, which is superior to those for the other five adsorption models. This confirms that, the nature of

adsorption is Langmuir adsorption which is uni-layer in character.

Langmuir adsorption is vital to recognize the relations between the green extract molecules and the MS surface. Constants for adsorption–desorption process (K_{ads}) and free

energy of adsorption (G_{ads}^0) are calculated from the Langmuir adsorption isotherm plot (Fig. 5). The obtained negative G_{ads}^0 values in the present investigation favorable for the adsorption process. The −ve sign in the G_{ads}^0 indicates a spontaneous adsorption phenomenon. The G_{ads}^0 values in the present investigation were between − 35 and − 37 kJ mol^{-1}. These values are between the literature values (around 20 kJ mol^{-1} = physical adsorption and around 40 kJ mol^{-1} = chemical adsorption). These supports both physical and chemical adsorption phenomena which are due to combined effect of the electrostatic interaction and sharing of electron between the charged plant extract species and the MS metal surface. The binding capacity of green corrosion inhibitor can be examined by K_{ads} values. The high K_{ads} values in acid system show more adsorption than desorption process and consequently higher protection efficiency. The obtained K_{ads} values also show that the MS corrosion in 3 M HCl solution takes place on the uncovered portion (MS surface not covered by organic species) of the MS surface (from Table 5).

Activation Parameters

Activation parameters (activation energy (E_a^*), activation enthalpy (ΔH^*) and activation entropy (ΔS^*) are vital for studying the nature of the interaction between the ES extract and the Mild steel. Ea* obtained from the below equation (Arrhenius plot; ln [corrosion rate] versus 1000/ T):

Fig. 6 Arrhenius plots
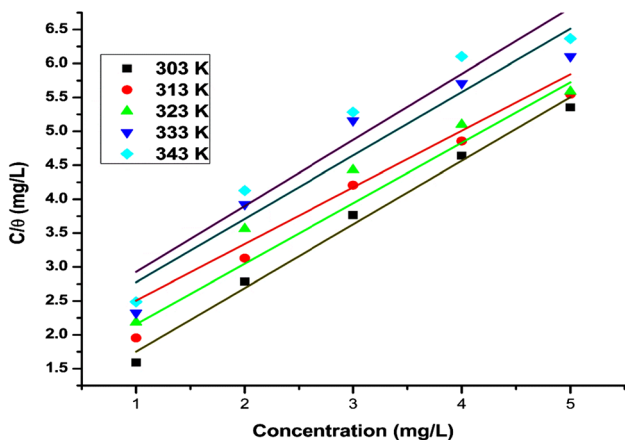

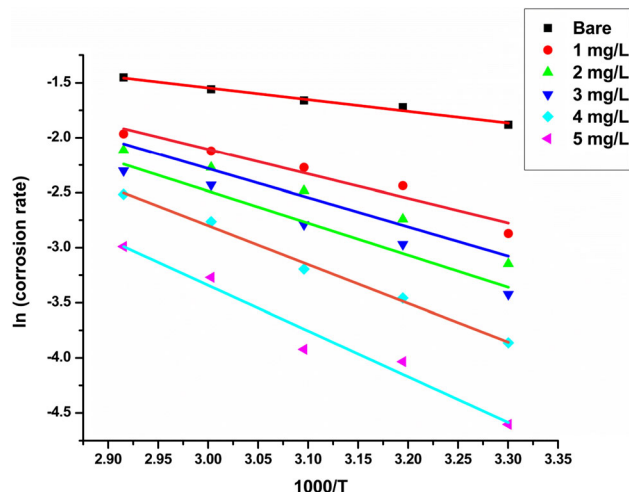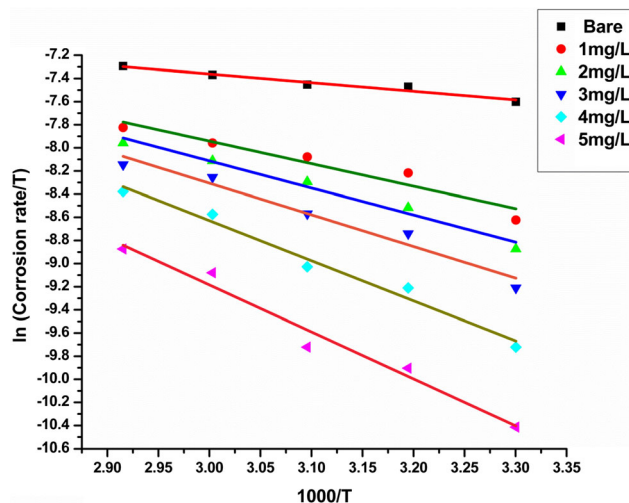
Fig. 5 Langmuir isotherm plot

Fig. 7 Transition state plots

Table 5 Thermodynamics parameters

Temperature (K)	Adj. R-square	Standard error (intercept)	Standard error (slope)	K_{ads} [L (mg)$^{-1}$]	ΔG_{ads}^0 (kJ mol^{-1})
303	0.98764	0.1738	0.0524	1231.026	− 35.333
313	0.97537	0.2342	0.07064	790.882	− 35.347
323	0.94627	0.3274	0.09872	598.465	− 35.728
333	0.90098	0.5068	0.15281	543.289	− 36.566
343	0.91024	0.5006	0.15096	511.765	− 37.494

966

J Fail. Anal. and Preven. (2021) 21:958–975

Table 6 Activation parameters for mild steel in 3 M HCl system

Adj. R-square		Concentration (mg/L)	E_a^* (kJ/mol)	A (kJ/mol)	ΔH^* (kJ/mol)	ΔS^* (J/mol/K)
Arrhenius plot	Transition state plot					
0.98099	0.94884	Bare	8.833	5.161	6.186	− 297.400
0.93317	0.91199	1	18.540	97.868	16.183	− 272.235
0.97163	0.97471	2	22.031	289.591	19.444	− 263.870
0.96754	0.95327	3	24.165	508.894	22.735	− 255.602
0.99267	0.97421	4	29.271	2348.424	28.796	− 240.111
0.95629	0.96443	5	34.504	9036.796	33.751	− 229.866

Table 7 AAS results

ES extract in mg/L (C)	Amount of MS dissolved in grams (W)	Degree of surface coverage (θ)	Protection efficiency in % (PE)
0	0.045	…	…
1	0.0226	0.497	49.777
2	0.0178	0.604	60.444
3	0.0123	0.726	72.666
4	0.0098	0.782	78.222
5	0.0013	0.971	97.111
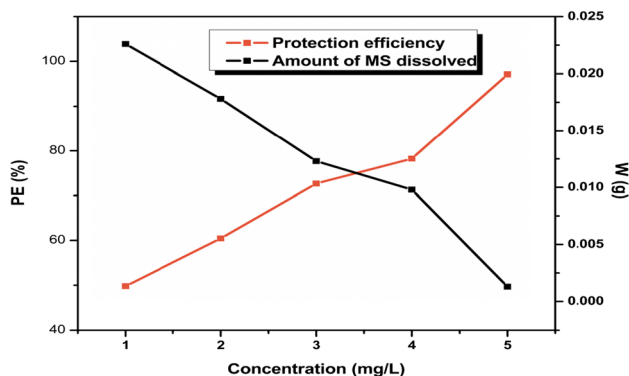
Fig. 8 Relation between the C, PE, and W in AAS results

Fig. 9 Tafel plots

$$\ln[\text{corrosion rate}] = \ln A - \frac{E_a}{RT}, \qquad \text{(Eq 4)}$$

where A = Arrhenius constant, and R = gas constant.

The activation enthalpy (ΔH^*) and entropy (ΔS^*) were calculated from the transition state relation (ln [corrosion rate]/T versus 1000/T:

$$\ln\frac{\text{Corrosion rate}}{T} = \left[\ln\frac{R}{Nh} + \frac{\Delta S^*}{R}\right] - \frac{\Delta H^*}{RT}, \qquad \text{(Eq 5)}$$

where N is Avogadro's number and h are plank's constant.

The results obtained from the Arrhenius plot (Figure 6) and transition state plot (Figure 7) is depicted in Table 6.
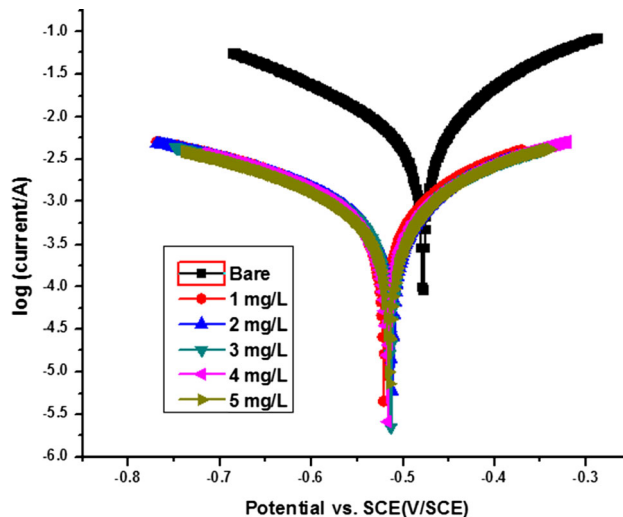
The link between the activation energy and solution temperature can be divided into following three divisions:

(a) If the protection efficiency has an inverse relationship with temperature, then activation energy in protected condition is greater than the unprotected condition.

(b) If the protection efficiency has a direct relationship with temperature, then activation energy in protected condition is less than the unprotected condition.

(c) If the protection efficiency does not change with temperature, then activation energy in protected condition is equal to than the unprotected condition.

In present investigation, the activation energy values for mild steel in 3 M HCl solution in the HCl solution was higher than the unprotected system and protection efficiency decreases with respect to solution temperature. This shows that the protective layer generated by ES extract on MS surface is electrostatic in nature (physical force of attraction). The difficulties in the mobility of H^+ and Cl^- ions occur at active MS surface due to the presence of an

Table 8 Tafel parameters

Concentration (mg/L)	E_{corr} (mV)	i_{corr} (A)	B_c (V dec^{-1})	βa (V dec^{-1})	Degree of surface coverage (θ)	Protection efficiency (%)
Bare	− 478	0.006300	5.79	7.18	…	…
1	− 521	0.0008433	4.838	5.731	0.86614	86.614
2	− 511	0.0008104	4.798	5.587	0.87136	87.136
3	− 513	0.0007642	4.916	5.675	0.87869	87.869
4	− 517	0.0007377	5.012	5.727	0.88290	88.290
5	− 515	0.0006920	5.017	5.719	0.89015	89.015

invisible barrier layer. Hence, the interaction between the MS surface and HCl solution decreases with a rise in the concentration of ES extract. As a result of this, more energy is required for the oxidation process. Adsorption effects lead to higher activation energy in the protected system compared to the unprotected system. In another way, the superior activation energy values explore the robust MS corrosion protection ability of ES extract. Therefore, MS surface is protected from the 3 M HCl solution by introduction of ES extract. Further, the activation enthalpy values are positive in both the systems (protected and unprotected), which is an indication of endothermic MS disintegration process in 3 M HCl solution. The disintegration of MS in acid system is difficult in the presence of five different concentrations of ES extract. Both activation enthalpy and energy values varying in the same fashion gives evidence for the anticipated MS corrosion protection mechanism. ΔS^* is another activation parameter that is higher in the ES extract than unprotected system. This clearly shows the dissociation process is the rate determining step. The disorderness reduces during reactants changes into activated complex. The activation entropy values are less negative compared with the blank system, indicating that the addition of five different amounts of ES extract to the 3 M HCl solution created near-equilibrium mild steel disintegration condition.

Atomic Absorption Spectroscopy (AAS) Results

The AAS technique of monitoring the protection efficiency is useful because of its reliability and simple application. The degree of surface coverage and protection efficiency of ES extract of five different concentrations is listed in Table 7. The effect of five different concentrations of ES extract is shown in Figure 8. It is seen that increasing ES extract reduces the amount of MS dissolved in the acidic medium, consequently enhancing both degree of surface coverage and protection efficiency. This nature could be related to the enhanced adsorption process of ES extract species at the electrode (MS)–electrolyte (3 M HCl) interface. The invisible protective layer blocks aggressive attack of H$^+$ and Cl$^-$ ions over the MS surface. The maximum protection efficiency 97.111 % was attained at 5 mg/L of ES extract. Further, a rise in the concentration of the ES extract did not show any significant variation in the protection efficiency values (not shown in Table 6). This nature is due to saturation state of ES extract species at MS surface.

Electrochemical Measurements

Polarization (Tafel plot) Study

Polarization curves of MS in 3 M HCl solution in the absence and presence of green compounds at five different concentrations at 303 K are shown in Fig. 9. All related parameters are listed in Table 8. The degree of surface coverage and protection efficiency was evaluated by using Eq. 4 and 5.

$$\text{Degree of surface coverage} = \left[1 - \frac{i'_{corr}}{i_{corr}}\right] \quad \text{(Eq 4)}$$

$$\text{Protection efficiency} = \left[1 - \frac{i'_{corr}}{i_{corr}}\right] \times 100, \quad \text{(Eq 5)}$$

where i_{corr}' = corrosion current densities in protected system, and i_{corr} = corrosion current densities in unprotected system.

Table 8 shows that, i_{corr} values in protected MS surface are low compared to the bare system. The decrease in i_{corr} values in protected system is due to the adsorption of green extract components on the MS surface. The adsorption layer on the MS surface in 3M HCl system prevents the

968

J Fail. Anal. and Preven. (2021) 21:958–975

diffusion of ions directed toward the MS metal. Table 8 also shows that protection efficiency increasing with the concentration of green extract molecules. This aspect is analogous to the results of weight loss technique. The change in the corrosion potential (E_{corr}), anodic Tafel slope (βa), and cathodic Tafel slope (βc) values showed that the adsorption of green organic species prevents the anodic dissolution and cathodic evolution processes. The shift in the E_{corr} values is not more than 85 mV in acid media, which clearly indicates the mixed corrosion inhibition property of the extract. This shows that, green extract molecules adsorb on both cathodic and anodic reactive sites.

Impedance Studies

Nyquist and bode diagrams that show the impedance characteristics of MS in 3 M HCl solution significantly varied with introduction of green chemicals are shown in Fig. 10a, b, and c. The Nyquist experimental and computed curves are shown in Figure 11. The various impedance parameters such as double layer capacitance (C_{dl}), CPE exponent (n), constant phase element (Q), frequency (f_{max}), Chi-squared value (χ^2), and resistance (R_{ct}) values are obtained as per procedure stated in previous reports [22]. Increasing the depressed semicircle curves with plant extract molecules indicates the adsorption and inhibitory modality of green extract species. ES extract decreases the 3 M HCl conductivity on the MS surface. Hence, MS is protected from disintegration process. The depressed semi circle also indicating the existence of charge transfer phenomena which are not affected by green molecules. The shape of the Nyquist diagrams is akin in bare and protected systems which show that protection efficiency of the ES extract on MS surface in 3 M HCl systems is related to the coverage ratio. All other parameters obtained from Nyquist plots support the corrosion protection role of ES extract. The results obtained from the Nyquist plots well supports the weight loss and Tafel plot technique results (Table 9).

Mathematical Views

In this case, how five different concentrations of ES extract and exposure time can affect both the protection efficiency (PE) and corrosion rate (CR) has been studied through the linear mathematical model. Generally, if the correlation coefficient is < 0.30, then the relationship between the two variables is very weak. The correlation coefficient between 0.50 to 0.70 indicates a moderate relationship between the
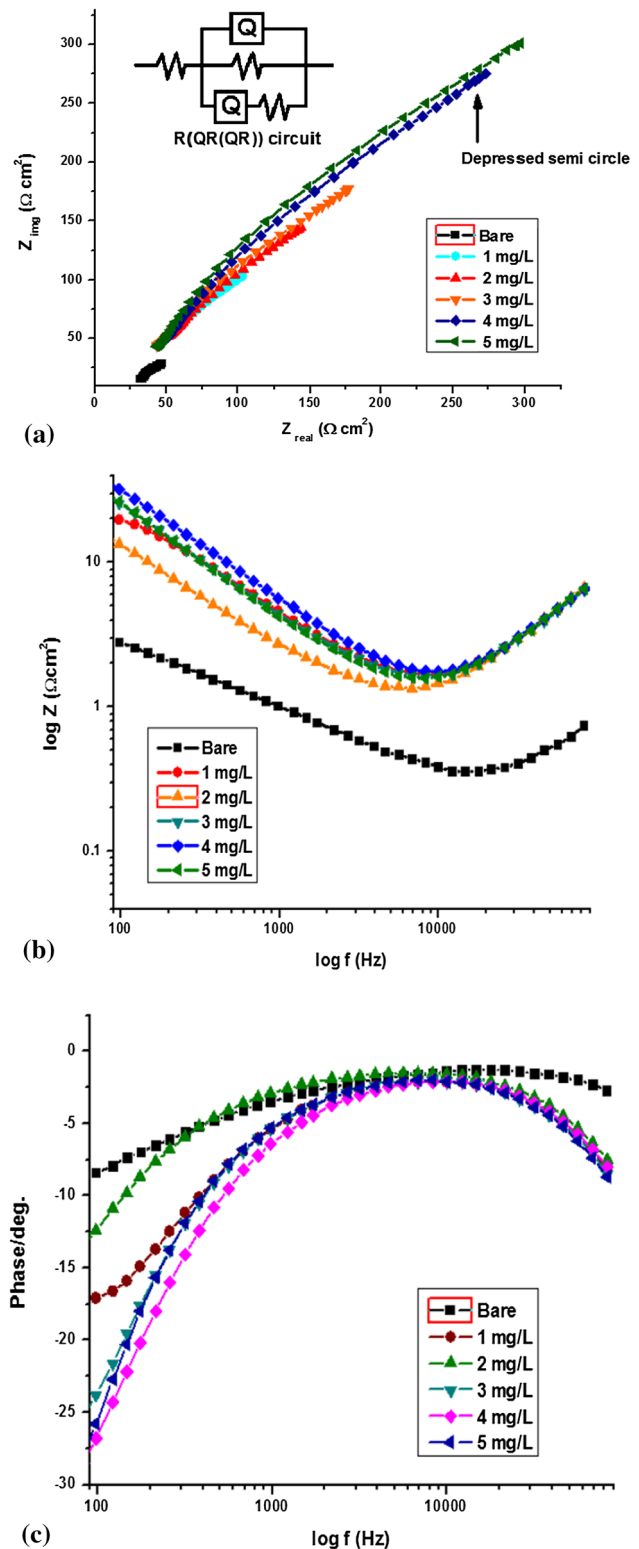

Fig. 10 Nyquist plots (**a**), bode plots (**b**) and bode phase angle plots (**c**)
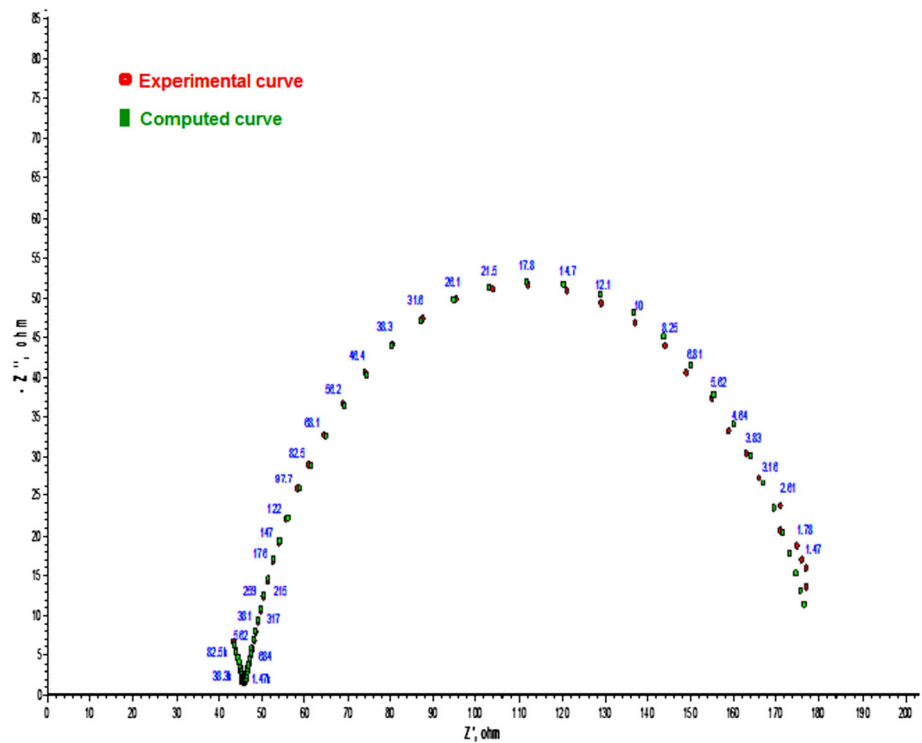
Fig. 11 Nyquist experimental and computed curves

Table 9 Impedance parameters

Concentration (mg L^{-1})	Q (Ω^{-1} µs^n)	N	R_{ct} Ω	C_{dl} (F)	τ (s)	χ^2	PE (%)
Bare	379.6	0.6806	30.13	2.458×10^{-4}	7.40×10^{-3}	6.991×10^{-5}	
1	0.063	0.8558	93.41	3.033×10^{-5}	2.83×10^{-3}	3.164×10^{-5}	67.744
2	0.052	0.8180	148.8	8.814×10^{-6}	1.31×10^{-3}	5.428×10^{-5}	79.751
3	0.041	0.8570	180.5	4.956×10^{-5}	8.94×10^{-3}	4.673×10^{-5}	83.307
4	0.022	0.9951	264.0	6.031×10^{-5}	15.92×10^{-3}	2.015×10^{-5}	88.587
5	0.038	0.8663	318.1	7.350×10^{-5}	23.380×10^{-3}	4.279×10^{-5}	90.528

two variables, whereas a correlation around 0.90 or close to unity signifies the powerful relationship between the two variables [23]. The linear regression carried out for protection efficiency and corrosion rate (obtained from weight loss technique) in protected and unprotected system in 3 M HCl at five different solution temperatures are shown in the below equations. Their respective plots are shown in Figure 12a, b, c, d, and e.
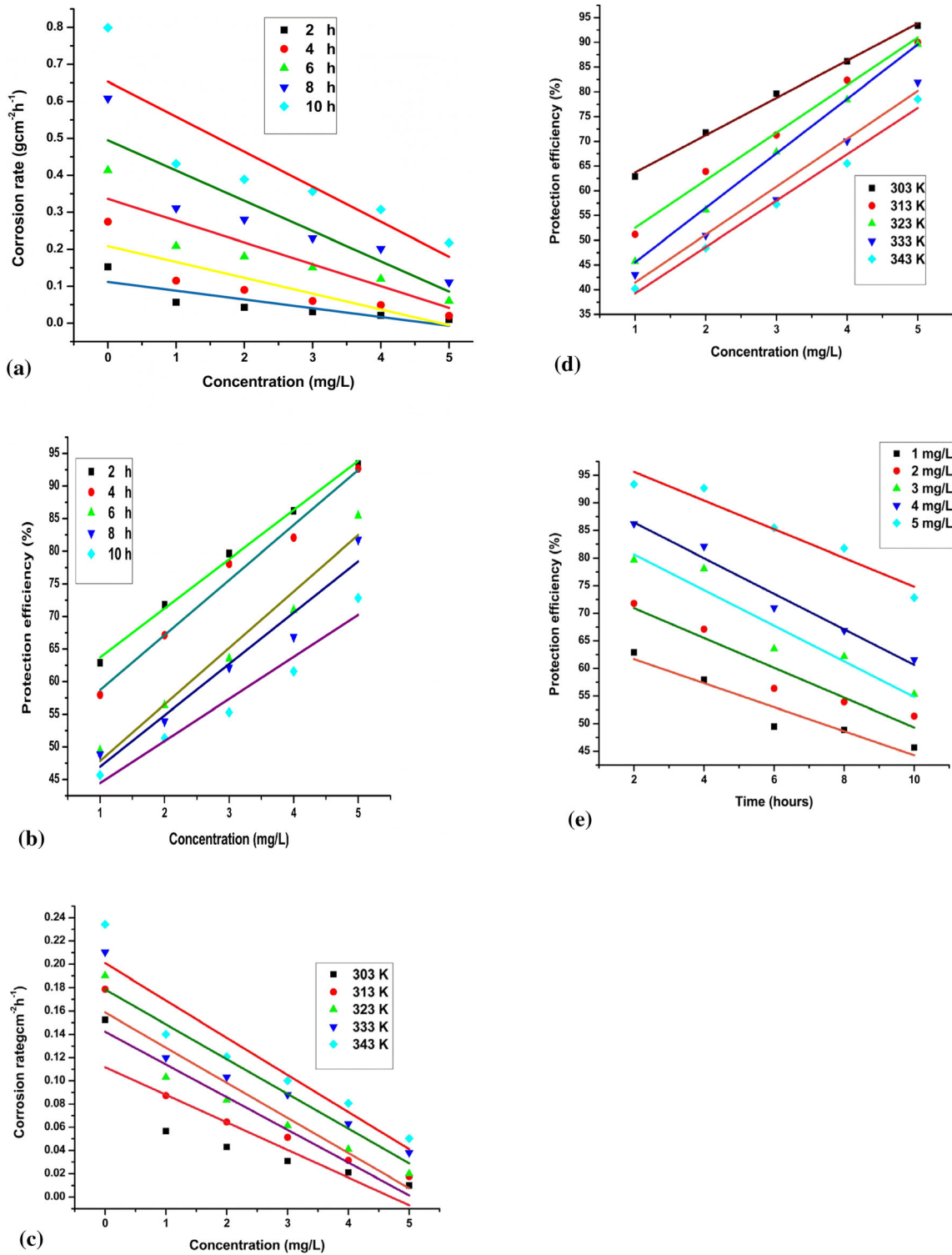
Fig. 12 Corrosion rate as a function of concentration (**a**), Protection efficiency as a function of concentration at 303 K (**b**), corrosion rate as a function of concentration (**c**), protection efficiency as a function of concentration at different solution temperatures (**d**), protection efficiency as a function of time at five different concentration of ES extract (**e**)

From Figure 12a : 2 h : $CR = 0.11173 - 0.02375 \cdot C \left(R^2 = 0.67315\right)$

4 h : $CR = 0.20864 - 0.04285 \cdot C \left(R^2 = 0.72331\right)$

6 h : $CR = 0.33616 - 0.05892 \cdot C \left(R^2 = 0.78141\right)$

8 h : $CR = 0.49478 - 0.08183 \cdot C \left(R^2 = 0.75879\right)$

10 h : $CR = 0.65328 - 0.09469 \cdot C \left(R^2 = 0.71750\right)$

From Figure 12b : 2 h : $PE = 56.1701 + 7.5357 \cdot C \left(R^2 = 0.99534\right)$

4 h : $PE = 50.2702 + 8.4368 \cdot C \left(R^2 = 0.98037\right)$

6 h : $PE = 39.1872 + 8.6586 \cdot C \left(R^2 = 0.96158\right)$

8 h : $PE = 39.095 + 7.8708 \cdot C \left(R^2 = 0.93905\right)$

10 h : $PE = 37.9921 + 6.4507 \cdot C \left(R^2 = 0.94596\right)$

From Figure 12c: 303 K: $CR = 0.11173 - 0.02375 \cdot C \left(R^2 = 0.67315\right)$

313 K : $CR = 0.14229 - 0.02817 \cdot C \left(R^2 = 0.789892\right)$

323 K : $CR = 0.1588 - 0.0302 \cdot C \left(R^2 = 0.85761\right)$

333 K: $CR = 0.17849 - 0.02991 \cdot C \left(R^2 = 0.8471\right)$

343 K : $CR = 0.20097 - 0.03197 \cdot C \left(R^2 = 0.8534\right)$

From Figure 12d : 303 K : $PE = 56.1701 + 7.5357 \cdot C \left(R^2 = 0.99534\right)$

313 K : $PE = 42.9024 + 9.6154 \cdot C \left(R^2 = 0.98978\right)$

323 K : $PE = 34.5473 + 11.0039 \cdot C \left(R^2 = 0.99963\right)$

333 K : $PE = 31.7638 + 9.6872 \cdot C \left(R^2 = 0.98196\right)$

343 K : $PE = 29.8666 + 9.3772 \cdot C \left(R^2 = 0.98802\right)$

From Figure 12e: 1 mg/L: $PE = 66.0271 - 2.17565 \cdot t \left(R^2 = 0.89502\right)$

2 mg/L: $PE = 76.3341 - 2.70375 \cdot t \left(R^2 = 0.90604\right)$

3 mg/L: $PE = 87.1349 - 3.23215 \cdot t \left(R^2 = 0.89775\right)$

4 mg/L: $PE = 92.8687 - 3.22345 \cdot t \left(R^2 = 0.96304\right)$

5 mg/L: $PE = 100.8164 - 2.5998 \cdot t \left(R^2 = 0.92031\right)$

From these plots, the reduction in the corrosion rate (CR) and elevation in protection efficiency (PE) with ES extract increases depending on five different solution temperatures (T) and immersion time (t). From these results, the correlation coefficients were greater than > 0.60 (concentration (C) versus corrosion rate) and > 0.93 (concentration versus protection efficiency) and > 0.89 (contact time versus protection efficiency) for the considered systems. These clearly show the good relationship between the two variables. Further, the below relations represent the mathematical model between corrosion rate and protection efficiency.

At 303 K: $PE = 99.91991 - 654.16801 \cdot CR \left(R^2 = 1\right)$

313 K: $PE = 99.92695 - 558.42949 \cdot CR \left(R^2 = 1\right)$

323 K: $PE = 100.14958 - 527.52642 \cdot CR \left(R^2 = 0.999\right)$

333 K: $PE = 100.00191 - 475.55855 \cdot CR \left(R^2 = 1\right)$

343 K: $PE = 99.99769 - 426.82409 \cdot CR \left(R^2 = 1\right)$

The mathematical views show a reduction in the MS disintegration rate with rise in ES extract concentration with decrease in the solution temperature and contact time, which shows a strong relationship between mathematical studies and weight loss studies.

Quantum Chemical Studies

The various quantum chemical properties of phytochemical compounds of ES extract computed from Argus Lab software are presented in Table 10 and Figure13. All the three compounds having high $-E_{HOMO}$ compared to $-E_{LUMO}$ values show effective corrosion protection property of catechin, gallic acid, and ellagic acid. These compounds have high tendency to donate electrons to vacant d-orbitals of the mild steel surface. The small energy gap ΔE

indicates high reactivity of ES extract; hence, high protection rate observed; this is because the energy required to remove the outer most orbital is low. All other quantum chemical parameters strongly support the experiential results for ES extract on MS surface in 3 M HCl solution.

Mechanism of Action

Corrosion inhibition of MS in 3 M HCl solution by the extract of ES can be thoroughly explained by molecular

Table 10 Quantum chemical parameters

Name of species	E_{HOMO} (eV)	E_{LUMO} (eV)	Energy gap (eV)	I	A	H	χ	Σ	μ	Ω
Catechin	− 8.87	− 2.07	6.80	8.87	2.07	3.40	5.47	0.29	− 5.4	4.39
Gallic acid	− 10.18	− 5.38	4.8	10.18	5.38	2.40	7.78	0.41	− 7.78	12.63
Ellagic acid	− 8.79	− 1.85	6.93	8.79	1.85	3.46	5.32	0.28	− 5.32	4.08

Fig. 13 Optimized structures, HOMOs and LUMOs of Main constituents of ES extract
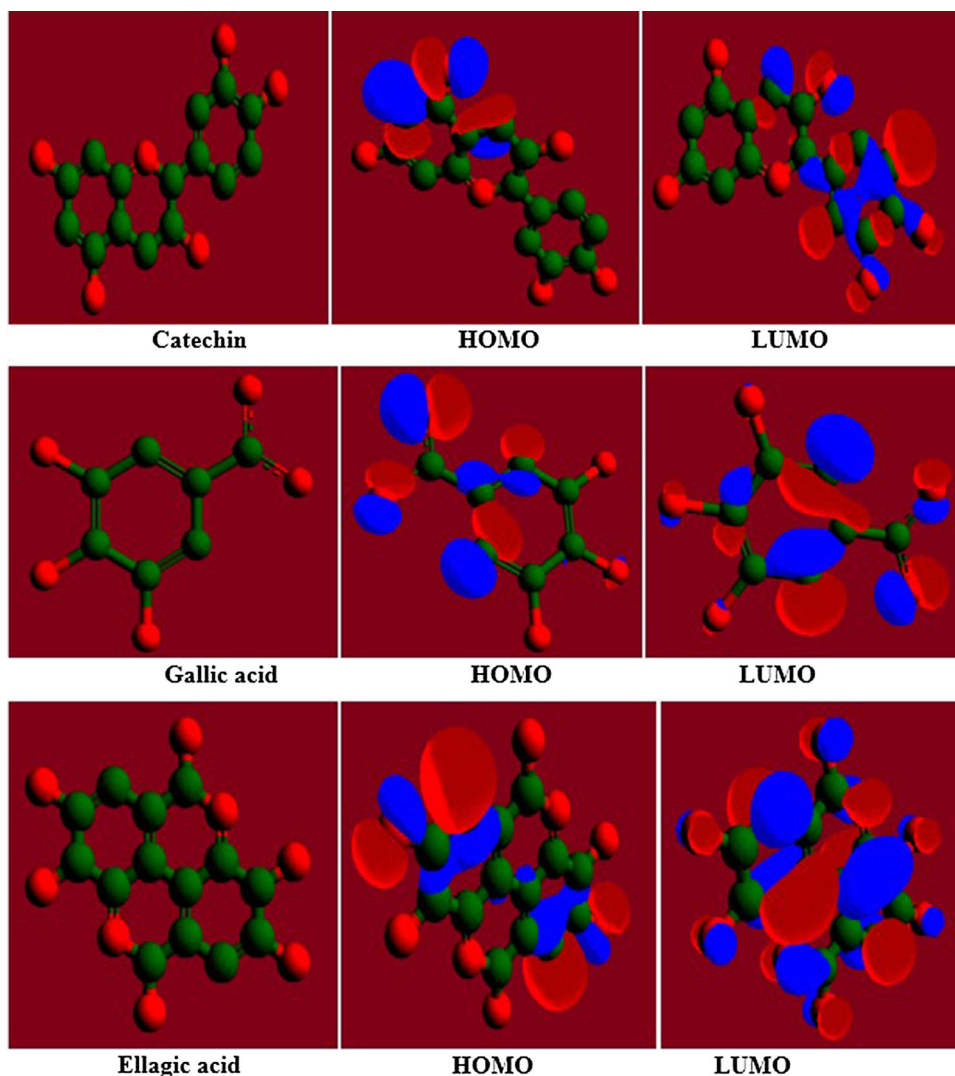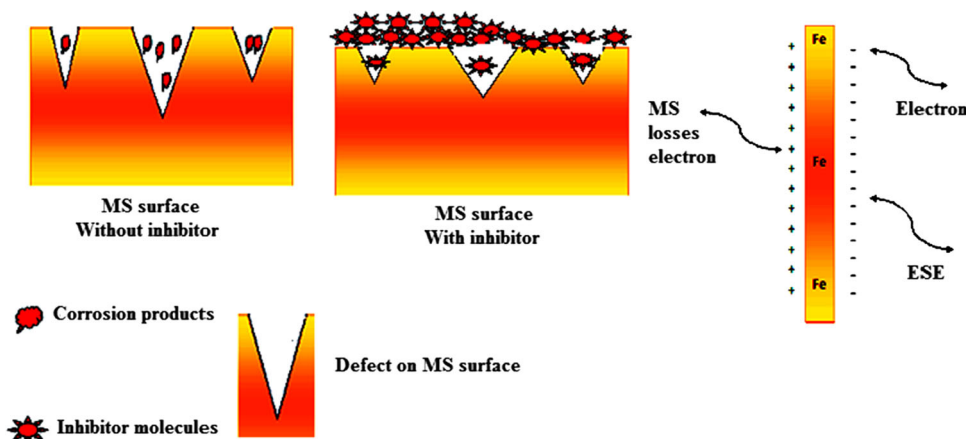
adsorption. The examined green compounds would have been adsorbed on the surface of MS as follows; donor–acceptor interaction occurs between the electrons of catechin, gallic acid , and ellagic acid and vacant d-orbitals of surface MS atoms. ES extract contains catechin, gallic acid, and ellagic acid as major components. In addition, it also contains a mixture of organic compounds in small amounts. Hence, it is difficult to decide the group that is responsible for the MS corrosion inhibition process. Therefore, the present study reports the combined effect all these compounds toward MS corrosion inhibition in 3 M HCl media. From the weight loss thermodynamic studies, it is revealed that adsorption of ES extract on MS surface in 3 M HCl involves comprehensive adsorption (both physical and chemical adsorption Fig. 14). Hence, MS corrosion inhibition in HCl media takes place via (a) electrostatic pure interaction existing between the ES extract molecules and MS metal or (b) transfer or sharing of electrons from ES to the MS surface in 3 M HCl media.

ES extract contains electron-rich species which possess electrons and lone-pair electrons in their moiety. The ES extract species exist as protonated species in a hydrochloric acid environment as follows:

$$ESE + xH \leftrightarrow [ESE - H_x]^{x+}$$
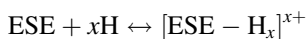
The ES extract components expected to adsorb on MS-HCl system interface by the following routes:

1. The protonated organic species of ESE adsorbed via electrostatic force of attractions with the positively charged MS surface by using the Cl⁻ ions which are attached to MS surface as negative species. After that, electrostatic interaction takes place between the electron-rich species of ES extract and d-orbital of MS surface, which leads to MS-inhibitor complexes as follows:

$$Fe \rightarrow Fe^{2+} + 2e^-$$

$$[ESE - H_x]^{x+} + Fe^{2+} \rightarrow [ESE - H_x - Fe]^{(2+x)+}$$
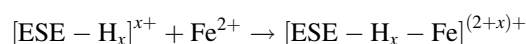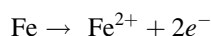
2. Neutral ligand species of ES extract adsorbed over MS surface through chemical bond mode, which involves displacement of H_2O species from the surface of MS. The ES extract species adsorbed over the MS surface by donor–acceptor interactions in between the electron-rich species and vacant d-orbitals of iron. The donor (ESE)-acceptor (Fe^{2+}) interactions can be represented as follows:

$$Fe \cdot H_2O_{(ads)} + ESE \rightarrow Fe \cdot ESE_{(ads)} + H_2O$$
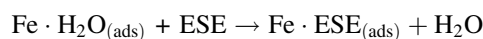
The presence of ES extract in 100 ml of 3 M HCl solution enhances the surface coverage of MS and hence there by high corrosion inhibition efficiency.

Comparison

The observed results from this investigation are reported in Table 11 for comparison purposes. It is observed from Table 11 that protection efficiency from weight loss technique is slightly different from the Tafel plot, impedance, and atomic absorption spectroscopy techniques. Weight loss method gives average corrosion inhibition efficiency values and the Tafel plot, impedance, and atomic absorption spectroscopy give instantaneous protection efficiency value. This is the main reason for the observed deviation in protection efficiency values. The high protection efficiency of ES extract is due to presence of π electrons, hydroxyl, and carbonyl groups in their organic species. ES extract compared with other natural inhibitors, and it is shown in Table 12.

974

J Fail. Anal. and Preven. (2021) 21:958–975

Table 11 Protection efficiency comparison obtained from different techniques

Optimum concentration (mg/L)	Protection efficiency (%)			
	Weight loss	AAS	Tafel plots	Impedance
5 mg/L	93.370	97.111	89.015	90.528

Table 12 Comparison of ES extract with other plant extract species

Inhibitor	Concentration	Metal	Protection efficiency (%)	References
Acalypha torta leaf extract	1000 ppm	Mild steel	91	24
Zenthoxylum alatum plant extract	2400 ppm	Mild steel	95	25
Rollinia occidentalis	1000 mg/L	Carbon steel	85	26
Griffonia simplicifolia	1000 mg/L	X80 steel	92	27
Arecanut husk	18 g/L	Mild steel	94	28
Areca fat	45 g/L	Mild steel	95	29
Areca flower	4 g/L	Carbon steel	87	30
Arecanut seed	4 g/L	Carbon steel	90	30
Cashew peel	800 mg/L	Carbon steel	80	31
Elaeocarpus seed	4 mg/L	Mild steel	97	Present paper

Conclusions

In our investigation the following conclusion can be drawn,

(a) Chemical weight loss studies show that ES extract acts as a green corrosion inhibitor for MS in 3 M HCl system and shows robust corrosion protection.

(b) Adsorption of ES extract on the MS surface in 3M HCl solution obeys the Langmuir isotherm model.

(c) Polarization study shows that the shift in corrosion potential value is less than 85 mv, hence, green ES extract acts as a mixed type in 3 M HCl solution by deactivating both the anodic and cathodic sites.

(d) Impedance studies confirm the adsorption property of the inhibitor and inhibit the MS disintegration process by charge transfer phenomena.

(e) Mathematical and quantum chemical results were in good agreement with the chemical and electrochemical results.

Conflict of interest Author Narasimha Raghavendra declares no conflict of interest.

References

1. D. Nestoridia, Pletcher, The study of aluminium anodes for high power density Al/air batteries with brine electrolytes. J. Power. Sour. **178**, 445–455 (2008)

2. E.M. Sherif, S.M. Park, Effects of 1, 4-naphthoquinone on aluminum corrosion in 0.50 M sodium chloride solutions. Electrochim. Acta. **51**, 1313–1321 (2006)

3. E.J. Lee, S.J. Pyun, The effect of oxide chemistry on the passivity of aluminum surfaces. Corros. Sci. **37**, 157–168 (1995)

4. R.T. Loto, Q. Tobilola, Corrosion inhibition properties of the synergistic effect of 4-hydroxy-3-methoxybenzaldehyde and hexadecyltrimethylammoniumbromide on mild steel in dilute acid solutions. J. King Saud Univ. Eng. Sci. (2016). https://doi.org/10.1016/j.jksues.2016.10.001

5. N. Raghavendra, J. Ishwara Bhat, Red arecanut seed extract as a sustainable corrosion inhibitor for aluminum submerged in acidic corrodent. Period. Polytech. Chem. **62**, 351–6358 (2018)

6. N. Chaubey, Y. Dk, V.K. Singh, M.A. Quraishi, A comparative study of leaves extracts for corrosion inhibition effect on aluminium alloy in alkaline medium. Ain Shams Eng. J. **8**, 673–682 (2017)

7. F.M. BinYehmed, A.M. Abdullah, Z. Zainal, Z.M. Ruzniza, Green coffee bean extract as a green corrosion inhibitor for aluminium in artificial acid rain medium. Int. J. Appl. Environ. Sci. **13**, 171–183 (2018)

8. N. Palaniappan, L. RajuChowhan, S. Jothi, I.G. Bosco, I.S. Cole, Corrosion inhibition on mild steel by phosphonium salts in 1M HNO3 aqueous medium. Surf Interface. **6**, 237–246 (2017)

9. M.H. Othman Ahmed, A.A. Al-Amiery, Y.K. Al-Majedy, A.A.H. Kadhum, A.B. Mohamad, T.S. Gaaz, Synthesis and characterization of a novel organic corrosion inhibitor for mild steel in 1 M hydrochloric acid. Results Phys. **8**, 728–733 (2018)

10. N. Raghavendra, J. IshwaraBhat, Green approach to inhibition of corrosion of aluminum in 0.5 M HCl medium by tender arecanut seed extract. Res. Chem. Intermed. **42**, 6351–6372 (2016)

11. N. Raghavendra, J. IshwaraBhat, Natural products for material protection: an interesting and efficacious anticorrosive property of dry arecanut seed extract at electrode (aluminum)–electrolyte (hydrochloric acid) interface. J. Bio. Tribo. Corros. **2**, 21 (2016)

12. A. Saxena, D. Prasad, R. Haldhar, Use of *Asparagus racemosus* extract as green corrosion inhibitor for mild steel in 0.5 M H2SO4. J. Mater. Sci. **53**, 8523–8535 (2018)

13. U.F. Ekanem, S.A. Umore, I.I. Udousoro, A.P. Udoh, Inhibition of mild steel corrosion in HCl using pineapple leaves (*Ananas comosus* L.) extract. J. Mater. Sci. **45**, 5558 (2010)

14. M. HazwanHussin, M. JainKassim, The corrosion inhibition and adsorption behavior of *Uncaria gambir* extract on mild steel in 1 M HCl. Mater. Chem. Phys. **125**, 461 (2011)

15. A. Singh, I. Ahamad, V.K. Singh, M.A. Quraishi, Inhibition effect of environmentally benign Karanj (*Pongamia pinnata*) seed extract on corrosion of mild steel in hydrochloric acid solution. J. Solid State Electrochem. **15**, 1087 (2011)

16. G. Ji, S.K. Shukla, P. Dwivedi, S. Sundaram, R. Prakash, Inhibitive effect of *argemone mexicana* plant extract on acid corrosion of mild steel. Ind. Eng. Chem. Res. **50**, 11954 (2011)

17. P.K. Dixit, S. Dixit, M. Bhardwaj, B. Chauhan, K. Nagarajan, J. Sahoo, A review on traditional and ethnomedicinal uses of *Elaeocarpus ganitrus*(Rudraksha). Int. J. Pharm. Sci. Rev. Res. **52**, 1 (2018)

18. G. Kumar, L. Karthik, K. Venkata, B. Rao, A review on medicinal properties of elaeocarpus ganitrus Roxbex. G.Don. (Elaeocarpaceae). Res. J. Pharm. Tech. **7**, 1 (2014)

19. J.Y. Bao, M. Cai, G. Sun, G. Wang, H. Corke, Anthocyanins, flavonoids and free radical scavenging activity of myrialrubia extracts and their color properties and stability. J. Agric. Food Chem. **53**, 2327 (2005)

20. N. Raghavendra, Theoretical approaches on the corrosion inhibition property of some important medicinal compounds against industrial imperative metals via computational methods. Res. J. Chem. Sci. **9**, 1 (2019)

21. N. Raghavendra, J. IshwraBhat, Application of green products for industrially important materials protection: an amusing anticorrosive behavior of tender arecanut husk (green color) extract at metal-test solution interface. Measurement. **135**, 625–639 (2019)

22. N. Raghavendra, Green compounds to attenuate aluminum corrosion in HCl activation: a necessity review. Chemistry Africa **3**, 21 (2020). https://doi.org/10.1007/s42250-019-00114-6

23. S. Boudhiba, K. Hanini, I. Selatnia, A. Saouane, M. Hioun, S. Benahmed, *Experimental, theoretical and mathematical studies of Echium italicum L. extract as a corrosion inhibitor for carbon steel in acidic medium*. (Res. Express, Mater, 2019) https://doi.org/10.1088/2053-1591/ab194f.2019

24. P.M. Krishnegowda, V.T. Venkatesha, P. Kumar, M. Krishnegowda, S.B. Shivayogiraju, *Acalypha torta* leaf extract as green corrosion inhibitor for mild steel in hydrochloric acid solution. Ind. Eng. Chem. Res. **52**, 722–728 (2013)

25. L.R. Chauhan, G. Gunasekaran, Corrosion inhibition of mild steel by plant extract in dilute HCl medium. Corros. Sci. **49**, 1143–1161 (2007)

26. P.E. Alvarez, M.V. Fiori, A. Bimbi, A. Neske, S.A. Brandán, C.A. Gervasi, Rollinia occidentalis extract as green corrosion inhibitor for carbon steel in HCl solution. J. Ind. Eng. Chem. **58**, 92–99 (2018)

27. E. Ituen, O. Akaranta, A. James, S. Sun, Green and sustainable local biomaterials for oilfield chemicals: *Griffonia simplicifolia* extract as steel corrosion inhibitor in hydrochloric acid. Sustain. Mater. Technol. **11**, 12 (2017)

28. N. Raghavendra, J.I. Bhat, Chemical components of mature areca nut husk extract as a potential corrosion inhibitor for mild steel and copper in both acid and alkali media. Chem. Eng. Commun. **205**, 145–160 (2018)

29. N. Raghavendra, J.I. Bhat, Chemical and electrochemical studies on the areca fat as a novel and sustainable corrosion inhibitor for industrially important materials in hostile fluid environments. J. Bio. Tribo. Corros. **3**, 12 (2018)

30. N. Raghavendra, Areca plant extracts as a green corrosion inhibitor of carbon steel metal in 3 M hydrochloric acid: gasometric, colorimetry and atomic absorption spectroscopy views. Mol. Eng. Mater. (2019). https://doi.org/10.1142/S2251237318500041

31. J.C. Rocha, J.A.C.P. Gomes, E. Delia, Corrosion inhibition of carbon steel in hydrochloric acid solution by fruit peel aqueous extracts. Corros. Sci. **52**, 2341 (2010)

Publisher's Note Springer Nature remains neutral with regard to jurisdictional claims in published maps and institutional affiliations.